THE JOURNAL OF PHYSICAL CHEMISTRY C
A JOURNAL OF THE AMERICAN CHEMICAL SOCIETY

pubs.acs.org/JPCC
Article

Molecular Description of Mechanical Structure−Property Relationships of Nanostructured Porous Carbon

Hemangi Patel, Jessica Kröner, Marina Schwan, Barbara Milow, and Ameya Rege*

Cite This: J. Phys. Chem. C 2024, 128, 21245−21252

ABSTRACT: A thermodynamic approach is proposed to model and simulate nanostructured porous carbon using all-atom molecular dynamics simulations. In this work, molecular dynamics models with a size of 800000 atoms have been developed and applied to analyze their mechanical structure−property relations. Models are generated for a wide range of densities (0.59−0.14 g cm^{-3}), which also represents the range of densities of the experimentally synthesized nanostructured porous carbon. The structural, fractal, and mechanical structure−property relations obtained are in good agreement with the experimental data from nanostructured porous carbon, as characterized from pore-size distributions, fractal dimension, surface area measurements, and uniaxial compression data. Insights into the effect of mechanical deformation on the pore morphology is provided. This study opens a platform for further developing and analyzing nanoporous carbon materials on a molecular scale for a wide range of applications.

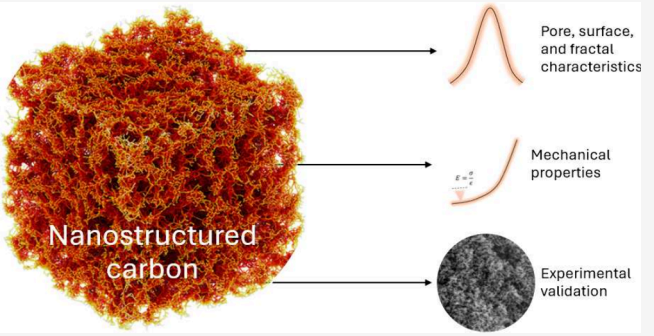

INTRODUCTION

Porous carbon materials present a ubiquitous solution to a diverse range of technological applications, like batteries, fuel cells, and supercapacitors, as sorbents for separation processes and gas storage, as well as acting as catalyst support.[1−4] Their unique physical and chemical properties, such as surface area, density, and electrical and thermal conductivity, account for their wide range of applications. One of the most distinctive features of nanoporous carbon materials is their high specific surface area that arises from their broad pore-size distribution in the microporous and mesoporous ranges.[5] In this context, carbon aerogels, with their large surface area, three-dimensional open-porous nanostructure, and low bulk density, have been extensively studied for their applications in batteries, supercapacitors, hydrogen storage, and as radiation adsorption material, to name a few.[1,3] They can be synthesized by carbonization of organic aerogels under inert gas conditions.[6] Although several experimental studies report on the development of such nanostructured porous carbon and carbon aerogels,[6−8] the atomic-scale phenomenon that plays a significant role in dictating these excellent properties remains to be understood. Computational modeling of nanostructured materials, including aerogels, along with their structure−property investigations have advanced significantly in the past decade. A summary of diverse mesoscale coarse-grained methodologies for modeling aerogels was reported recently by Rege.[9] On a lower scale, considering atomistic degrees of freedom, molecular dynamics (MD) has been extensively exploited to model nanoporous materials including nanostructured silica,[10−12] however very few studies have reported on all-atom description of carbon aerogels or porous carbon so far.[5,13] Aside from all-atom MD studies, coarse-grained models combined with Monte Carlo simulations have been employed to study diverse aspects in nanoporous carbon, particulary adsorption.[14−16] The adsorption behavior in mesoporous carbon was furthermore studied applying density functional theory-based approaches.[17,18]

In this work, we report on method development and mechanical structure−property analysis of nanostructured networks of porous carbon using an all-atom molecular dynamics simulation approach. The goal was to develop an approach for designing nanostructured porous carbon that mimics the behavioral characteristics of carbon aerogels. The subject of this article focuses on the structural features, namely, the pore-size distributions and surface area, and its influence on the fractal and mechanical properties. The results also elaborate on the flexibility of the porous carbon material, in particular, with respect to the pore sizes.

The paper is organized as follows. The Materials and Methods section outlines first the experimental procedure for

Received: October 22, 2024
Revised: November 15, 2024
Accepted: November 19, 2024
Published: November 29, 2024

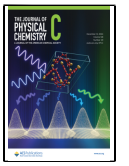

https://doi.org/10.1021/acs.jpcc.4c07159
J. Phys. Chem. C 2024, 128, 21245−21252

Table 1. Experimental Synthesis Conditions Used to Prepare Carbon Aerogels with Varying Densities[a]

density (g cm^{-3})	R:C	R:W	R:F	pH	stirring time (min)	gelation time (days)	drying	carbonization
0.225	200	0.012	0.5	7.1	30	7	sc-CO_2	1000 °C, 1 h, Ar
0.196	200	0.009	0.5	7.1	30	7	sc-CO_2	1000 °C, 1 h, Ar
0.137	200	0.019	0.5	6.5	30	7	sc-CO_2	1000 °C, 1 h, Ar; 900 °C, 2 h, CO_2

[a]Note: pH was measured in the initial solution.

developing the carbon aerogels and different analytical methods used to characterize their properties. This is followed by insights into the modeling methodology for designing nanoporous carbon at the atomistic level. The Results section first outlines the results from experimental characterization. This is followed by an illustration of the results from the model results, and a discussion on their validation is presented. A conclusion is presented at the end, giving an outlook into further potential studies based on this work.

MATERIALS AND METHODS

Experimental Section. Carbon aerogels are highly nanostructured micro- and mesoporous materials, those that are typically obtained by carbonizing organic aerogels. Within the scope of this paper, phenolic-based aerogels from resorcinol and formaldehyde were synthesized by the sol−gel process, followed by solvent exchange for removal of residues and preparation for drying, subsequently followed by drying under supercritical conditions. The following carbonization was carried out in an electric furnace by using argon. The experimental procedure and characterization techniques are outlined in the following.

Synthesis of Resorcinol Formaldehyde Aerogels. Resorcinol (R) was dissolved at room temperature in deionized water (W) under stirring at 150 rpm using a cross-magnetic stirring bar (Table 1). An aqueous solution of formaldehyde (F) and solid sodium carbonate is then added to the stirred resorcinol solution. The pH value of the RF solution was adjusted with 2 N nitric acid for the sample with a final density of 0.137 g cm^{-3}. For the other two densities, 0.196 and 0.225 g cm^{-3}, the pH value was not changed. Stirring at room temperature was continued for 30 min, and the homogeneous transparent solution was placed in a sealable polypropylene container in an oven at 60 °C (Memmert GmbH, Germany). After 7 days of gelation and aging, the wet gels were cooled down to room temperature and transferred into an acetone bath in order to remove residual reagents and to exchange water by acetone being soluble in supercritical carbon dioxide. The acetone was refreshed six times within 3 days. The supercritical drying was carried out with CO_2 in an autoclave of 60 L volume (Eurotechnica, Germany) at 60 °C and 110 bar for about 21 h. The degassing rate was adjusted to 0.2 bar·min^{-1}.

Carbonization. The carbonization was carried out in an electric furnace (KS-3-80-Vac-Sonder, Linn High Therm, Germany) using argon. The resulting RF aerogels were placed in the furnace, purged three times with argon, and heated to a carbonization temperature of 1000 °C. The heating rate was adjusted to 5 K min^{-1}, and the pressure was adjusted to 50 mbar. The temperature was kept for 60 min, whereupon the samples, carbon aerogels, were cooled down to room temperature under an inert atmosphere.

The subsequent activation of the aerogel with a density of 0.137 g cm^{-3} was performed in an electric furnace (Standardofen "F(A)", Gero Hochtemperaturöfen GmbH, Germany) using CO_2. The carbon aerogel was placed in the furnace, purged three times with argon, and heated to the activation temperature of 900 °C. The heating rate was adjusted to 400 K h^{-1}, and the pressure in the oven was adjusted to 50 mbar. After the activation time (2 h) at these conditions, the sample was cooled down to room temperature.

Characterization of Carbon Aerogels. The microstructure of the aerogels was investigated by using a scanning electron microscope (Zeiss Merlin, Germany). In preparation, all aerogels were coated with platinum for 90 s with 16 mA. The bulk densities were measured using a GeoPyc instrument based on a displacement measurement technique (Micromeritics, Germany). For physisorption experiments, the samples were degassed for 12 h at 200 °C and 0.1 to 0.5 mbar (SmartVacPrep, Micromeritics, Germany). The measurements of specific surface area, meso- and micropore size distribution, mesopore volume, and micropore volume were performed at 77 K by nitrogen adsorption−desorption isotherms (3Flex, Micromeritics, Germany). The calculations were based on the BET/BJH/DFT/t-plot methods. For the t-plot and BJH, a Carbon Black STSA model was used.

Molecular Dynamics Simulations. The main challenge lies in representing this nanostructure at the molecular level. While there have been reports on representing 3D graphene networks,[19] to the best of the knowledge of the authors, no reports on all-atom description of nanostructured carbon has been reported. Since the goal of this study was not to mimic the synthesis process of the nanostructured carbon but to merely provide a relevant topological description, it would be safe to assume describing pure carbon-based systems. Thus, the Adaptive Intermolecular Reactive Empirical Bond Order (AIREBO) potential was found to be a suitable choice for a force field, given that it accounts for the long-range, short-range, and dihedral interactions occurring in hydrocarbons and has been previously reported to accurately describe purely carbon-based materials.[19,20] Mathematically, the potential is given by

$$E = \frac{1}{2}\sum_{i}\sum_{j\neq i}\left[E_{ij}^{\mathrm{REBO}} + E_{ij}^{LJ} + \sum_{k\neq i,j}\sum_{l\neq i,j,k} E_{kijl}^{\mathrm{TORSION}}\right] \quad (1)$$

The E^{REBO} term in the AIREBO potential gives the model its reactive capabilities and describes short-ranged C−C interactions ($r < 2$ Å). These interactions have strong coordination-dependence through a bond order parameter, which adjusts the attraction between the i, j atoms based on the position of other nearby atoms and thus has 3- and 4-body dependence.[21] The E^{LJ} term adds longer-ranged interactions ($2 < r <$ cutoff) using a form similar to the standard Lennard-Jones potential. The E^{LJ} term in AIREBO contains a series of switching functions so that the short-ranged Lennard-Jones (LJ) repulsion ($1/r^{12}$) does not interfere with the energetics captured by the E^{REBO} term. The extent of E^{LJ} interactions is determined by the cutoff argument to the pair style command, which is a scale factor. The E^{TORSION} is the four-body term that

https://doi.org/10.1021/acs.jpcc.4c07159
J. Phys. Chem. C 2024, 128, 21245−21252

describes various dihedral angle preferences in hydrocarbon configurations.

The model development and simulations were carried out on the Large-scale Atomic/Molecular Massively Parallel Simulator (LAMMPS).[22] As a first step, 800000 carbon atoms were initialized and randomly distributed in a simulation box of 30 nm. This system has a density of 0.591 g·cm^{-3}. This highly disordered system is equilibrated for 25 ps under constant-temperature and constant-pressure (NPT) conditions. An amorphous carbon structure is obtained by subjecting the system to a high temperature of 5000 K for 25 ps and kept at this high temperature for 25 ps before being cooled back to 300 K at constant-temperature and constant-volume (NVT) conditions and equilibrated for 25 ps at NPT conditions. The schematic is shown in Figure 1a. The resulting

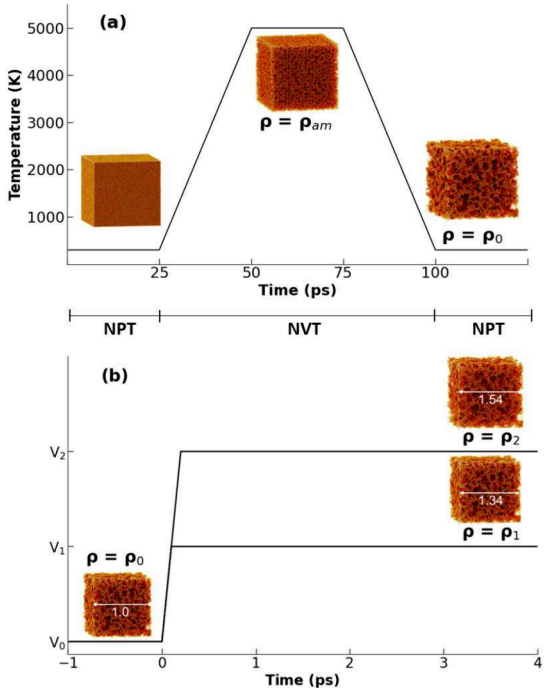

Figure 1. Thermodynamical approach to model porous nanostructured carbon. (a) The annealing treatment was applied to generate amorphous and nanostructured porous carbon; (b) The expansion method was applied to induce porosity in the nanostructured carbon, exemplarily illustrating models with 1.34× and 1.54× expansions in comparison to the preliminary porous structure.

structure is then allowed to relax under stable pressure conditions. At this point, formation of an initial structure of clustered network of carbon is observed as represented by Figure 1a. This initially formed network of voids and clusters (V0) serves as a starting point for the formation of micro- and mesopores on instantaneous expansion and subsequent NPT−NVT equilibration cycles, as represented in Figure 1b, to obtain structures of lower densities, calculated from the subsequent volumes V1 and V2. On instantaneous expansion for 0.7 ps and subsequent equilibration, the nanostructured network of desired density can be obtained. These expansion steps are carried out as shown in Figure 1b. It is worth noting that the equilibration plays a major role in allowing the atoms to regain the most energetically favorable positions.

RESULTS AND DISCUSSION

Experimental Section. The microstructure of the carbon aerogels was investigated by using a scanning electron microscope. Exemplary images of the nanostructured carbon synthesized in our lab are illustrated in Figure 2a.1−a.3. Diverse characteristics, such as the density, specific surface area, pore-size distribution, and mesopore volume, were investigated.

The pore-size distribution was obtained as follows. Physical gas sorption was performed on the exemplary aerogels, and the isotherms during adsorption and desorption were exported as illustrated in Figure 2b.1. DFT analysis[23] and BET/BJH were performed on the desorption isotherms, and the pore-size distributions were obtained. These are demonstrated in Figure 2b.2, which shows a small peak at approximately 1 nm and sharp peaks between 50 and 100 nm. At lower densities (0.137 g cm^{-3}), a wide peak is observed between 20 and 100 nm, indicating a wider distribution of pore sizes compared to the samples at higher densities where the pores are more or less uniformly distributed in the mesoscale range. This also aligns well with the SEM images which show the particles distributed uniformly at higher densities and more clusters at lower densities. The synthesized aerogels were subjected to uniaxial compression for extracting their mechanical properties. Figure 2(c) demonstrates the stress−strain curves of all the synthesized aerogels, and one can already observe the significant influence of the density on not only the linear elastic regime of the stress−strain curve but also the large deformations in the network. This dependence can be quantified by means of a power law.[24] While aerogels exhibit an exponent between 2 and 4, these particular nanostructured carbon materials demonstrate an exponent of precisely 2.40 ± 0.05. This is close to the quadratic relation as mathematically derived by Gibson and Ashby, which can be attributed to their high network connectivity.[25]

Computational. A further investigation on the geometric, structural, and mechanical properties of the model porous carbon systems is carried out on energetically stable networks over a wide range of densities: 0.591, 0.331, 0.269, 0.196, and 0.144 g cm^{-3} are obtained. Experimentally, carbon aerogels were prepared with densities in a similar range.

Once the MD models of nanoporous carbon are completely simulated, their visualization is done using OVITO. A first impression of the morphology of the structure after expansion and subsequent minimization reveals that, although the cluster sizes do not change considerably, the void volume increases. This agrees well with diverse experimental reports,[7,8,13] that with changing density, on the one hand, the pore diameter (void) changes respectively, but on the other hand, the particle diameter or the pore-wall width has a marginal to negligible effect. Another noticeable structural evolution is the reduced connectivity of the clusters with the decreasing density giving rise to pore size formation from the micropore to mesopore range.

Radial distribution function (RDF) $g(r)$ for configurations with densities ranging from 0.591, 0.331, 0.269, 0.196, and 0.144 g cm^{-3} are plotted in Figure 3a. A single frame is used to calculate the RDF which is reported to be sufficient for a large number of atoms.[26] In general, there is a clear gap between the first nearest neighbors (1.4 Å) and the second nearest neighbors (2.4 Å), which becomes sharper at lower densities. This indicates a strongly ordered structure. The peak positions

https://doi.org/10.1021/acs.jpcc.4c07159
J. Phys. Chem. C 2024, 128, 21245−21252

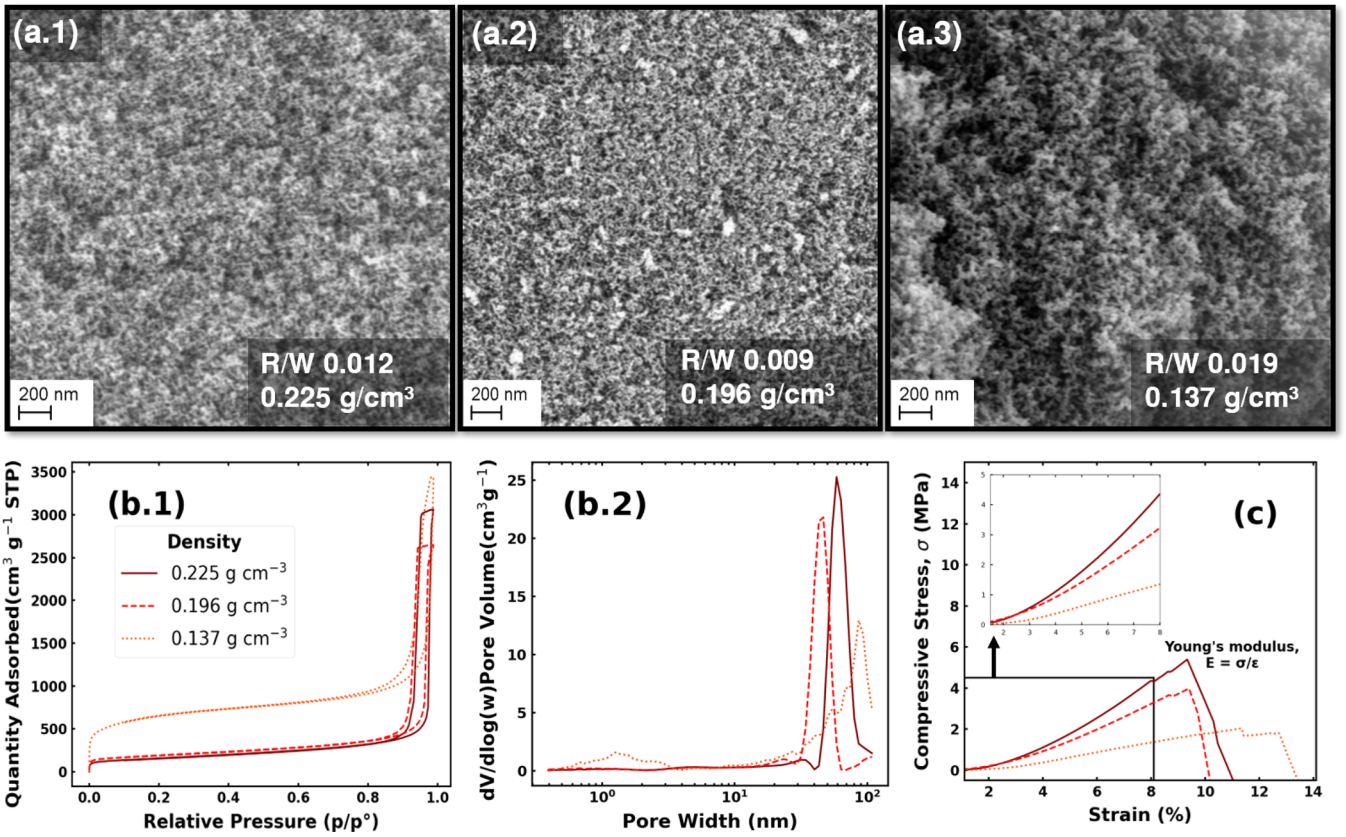

Figure 2. (a) Scanning electron micrographs illustrating the nanostructured porous morphology of carbon aerogels with varying densities, namely, (a.1) 0.225, (a.2) 0.196, and (a.3) 0.137 g cm^{-3}. (b.1) Isotherms from nitrogen sorption measurements, (b.2) pore-size distributions, and (c) stress−strain curves from uniaxial compression measurements.

observed at 1.4, 2.4, and 2.6 Å correspond to the clustered carbon network of graphitic nature. This agrees well with the observations reported by Wang et al.[13]

To investigate the surface and pore characteristics, the all-atom model is converted to a surface model in OVITO. The surface model is demonstrated in Figure 3b. The results from the surface area are illustrated in Figure 3c. One can observe the decreasing surface area with increasing density. This aligns well with the experimental results obtained from the BET measurements. The surface to volume ratio increases with increasing density. Furthermore, the pore space is quantified by calculating the pore-size distributions. These are illustrated for the modeled carbon structures in Figure 3d. One must note that the surface area and pore size calculations are from the modeled pore width range between 1 and 60 Å. This range coincides with the pore sizes in the microporous and very small pores from the mesoporous range. Thus, quantitative validation with the aerogels does not make sense, but the qualitative trends agree very well with our experiments and the reported available literature. Interestingly, one can compare the pore-size distribution exemplarily of the nanostructured porous carbon, model and the aerogel, having a density ≈0.14 g cm^{-3}. One can observe that the model peak and the experimental peak from DFT nearly coincides. The frequency of the modeled carbon is significantly higher, as the model covers a range only up to 60 Å, while the experimental characterization explores the entire mesoporous space (up to 500 Å).

Silica aerogels are known to exhibit a fractal nature.[27] Pekala[7] carried out small-angle scattering measurements on carbon aerogels and reported that they exhibit no fractal nature. Fractal properties can be quantified by the fractal dimension. The box counting method is typically used to characterize the fractal dimensions for 3D geometric structures. The process is well-known in the modeling literature investigating fractal dimension in silica aerogels.[28,29] Figure 4 illustrates this approach. The center of the model box is chosen as the starting point, and at every iteration, a sphere with increasing radius is drawn, and the number of atoms (representative of the mass for same type of atoms) is calculated at every iteration. These are plotted as shown in the Figure 4. The slope of the curve is the fractal dimension. The measured value for our nanostructured porous carbon is 2.97. This is very close to 3.0, which is then the Eucledian dimension for a 3D material system. As the fractal dimension approaches 3.0, the structures become nonfractal, as observed in our case. On the other hand, silica aerogels exhibit highly fractal structures with a fractal dimension between 1.8 to 2.4.[30] To this end, our model captures the nonfractal nature of the representative carbon aerogels. Furthermore, the illustration of the surface, pore, and fractal characteristics along with the inferences from the RDF demonstrate the applicability of the AIREBO interatomic potential in describing the nanostructure of porous carbon.

While the RDF, surface characteristics, pore-size distribution, and fractal dimension of the model already provides an insight into the structure of the nanoporous network, their flexibility and strength can be numerically determined from mechanical characterization. Mechanical properties of the nanostructured carbon network, primarily, elastic modulus was estimated by simulating uniaxial compression to be

https://doi.org/10.1021/acs.jpcc.4c07159
J. Phys. Chem. C 2024, 128, 21245−21252

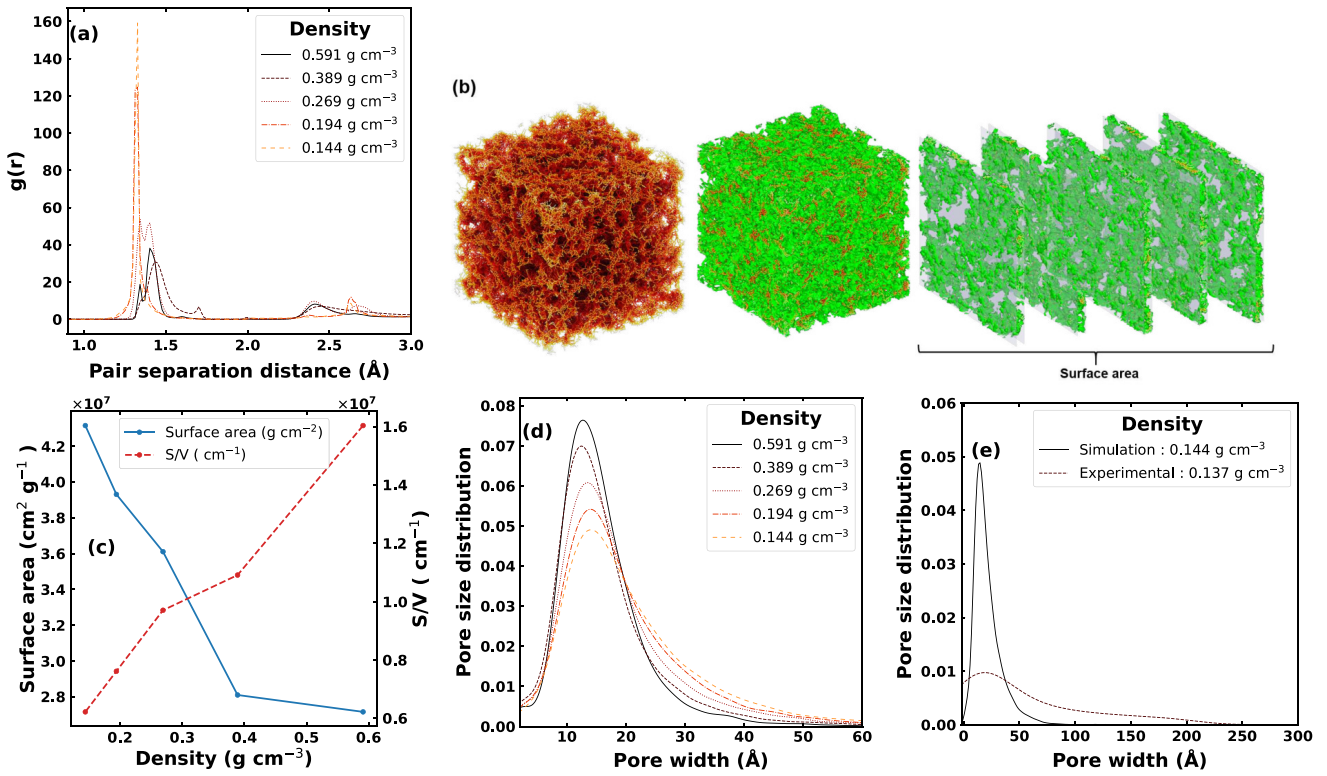

Figure 3. (a) Radial distribution function diagrams of the model carbon structures, (b) surface construction on the all-atom carbon model and slices showing the porous morphology, (c) surface area and surface-to-volume calculations made from image analysis in OVITO, (d) pore-size distributions of the model carbon structures, and (e) comparison of the pore-size distribution of the modeled porous carbon and the experimental aerogel of density ≈ 0.14 g cm^{-3}.

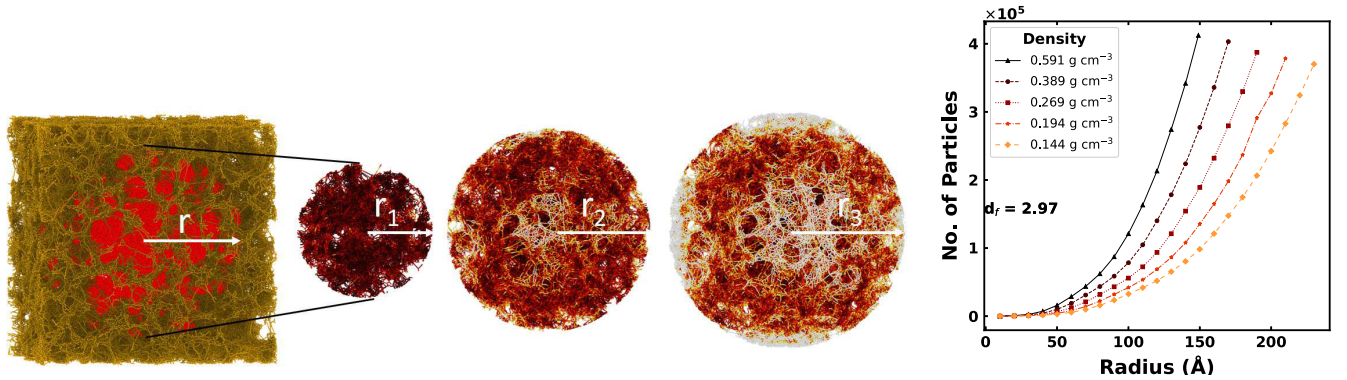

Figure 4. Box method used to characterize the fractal properties of the modeled nanostructured carbon and the results showing the nonfractal nature of these materials as demonstrated by a fractal dimension of 2.97.

consistent with the experimental output. The model aerogels were compressed using a time-step size of 0.5 fs and using an NPT ensemble under atmospheric conditions. The elastic modulus was determined from the slope of the linear region under small deformation. As the strain rate has considerable effect on the mechanical properties like yield strength of a material an optimal strain rate of 0.0025 ps^{-1} was chosen to perform compression, thus mimicking quasi-static behavior. Literature also suggests experimentally prepared carbon aerogels as robust, glassy, and brittle, with great stiffness. Figure 5a,b exemplarily shows the process of uniaxial compression of nanostructured carbon having a density of 0.269 g cm^{-3}. The density of the structure significantly affects the mechanical properties of the material. In low-density structures, the spatial arrangement of atoms changes with decreasing densities as atoms move apart from each other, thus increasing the void volume. An increase in the densities results in a higher resistance to the compression of voids due to the resistance from larger clusters. This in turn leads to the early densification and the stiffer stress−strain response.

Figure 5c shows the stress−strain curves at three densities, 0.269, 0.194, and 0.144 g cm^{-3}, computed under uniaxial compression. These particular densities of nanoporous carbons were selected, which are comparable to the experimentally synthesized carbon aerogels. The graph shows the stress−strain curves with a maximum compression of 25%, and the initial linear regime was considered for studying the relationship between the elastic modulus (E) and density (ρ). There was a significant decrease in the elastic modulus with the decreasing density. The resulting relationship between E and ρ

https://doi.org/10.1021/acs.jpcc.4c07159
J. Phys. Chem. C 2024, 128, 21245−21252

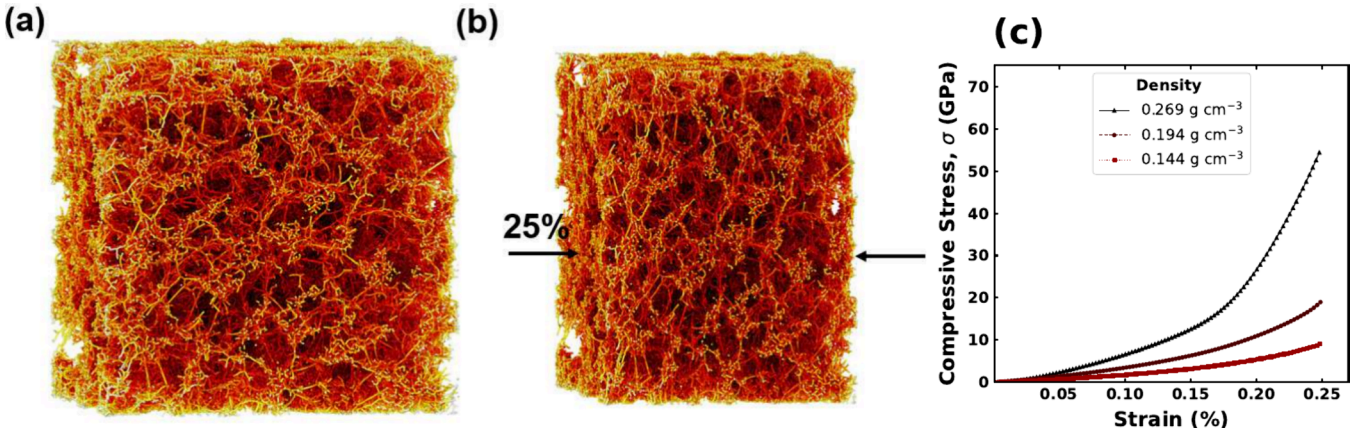

Figure 5. (a) Reference morphology of the modeled nanostructured carbon, (b) deformed morphology of the same structure, and (c) stress−strain curves from uniaxial compression of the model nanostructured porous carbon.

can be described by a power law. In our study, the exponent was found to be 2.20 ± 0.05. The comparison between the model and experimental results is tabulated in Table 2.

Table 2. Scaling Exponent Is Derived from Experimental Compression Curves and That from the Molecular Dynamics Model

	exponent
experiment	2.40 ± 0.05
model	2.20 ± 0.05

This computed value of the exponent is close to the experimentally found one, 2.40 ± 0.05, with an error bar of <10%. Thus, the proposed model of the porous carbon network is in good agreement with the experimental work on stiff carbon aerogels. Comparing the computational and macroscopic mechanical behavior leads to the following conclusions. The failure under compression of the nanostructured carbon (aerogel) is not due to skeletal material features at the molecular scale but rather those at the microstructural one. These could be existing cracks during synthesis, prestress due to drying the aerogels, macroporous voids during solvent exchange or extraction. This also explains the computationally obtained scaling exponent being more close to the quadratic relation than that obtained from experimental macroscopic compression of the nanostructured network, which would involve the above-mention uncertainties accounting for loss of or poorer connectivity compared to the molecular picture. This also explains the differences in the magnitude of the stresses arising at the molecular level and at the bulk level. At the molecular level, primarily the bonded interactions between the carbon atoms are responsible for the mechanical forces. On the other hand, at the bulk level, these along with the internal artifacts, internal cracks arising from stress concentrations developed during supercritical drying of the samples, and the range of pore sizes (Å to hundreds of nm) all affect the stresses and the resulting mechanical properties, e.g., Young modulus. These observations have also been made in the case of porous nanostructured silica.[12]

Furthermore, the effect of compression on the pore sizes was analyzed. Few pores having pore sizes between 10 and 60 Å were chosen (Figure 6a). These pores were analyzed before and after compression, and the results are illustrated in Figure 6b. It can be observed that the largest pore having a pore size of 60 Å deformed by about 20% in volume after compressing it to 25% strain. This was also observed for pores of about 40−50 Å. On the other hand, the smaller pores between 10 and 20 Å

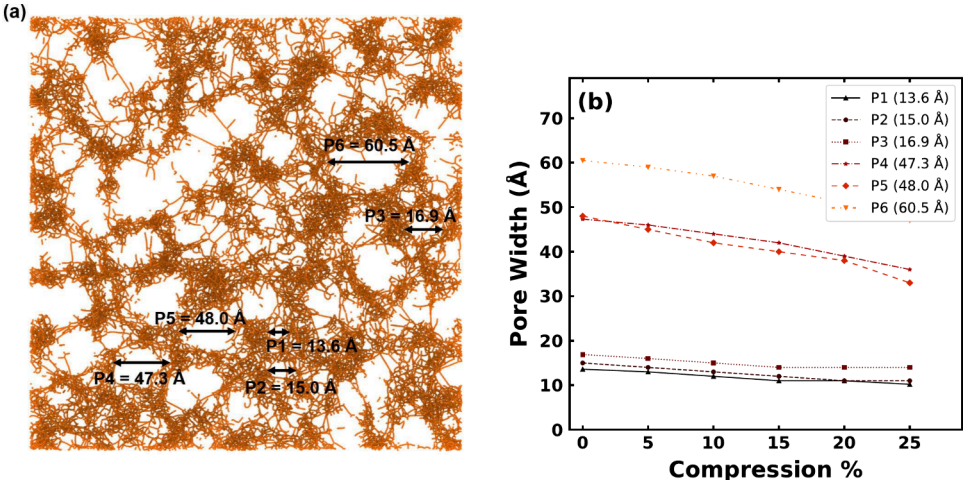

Figure 6. (a) Exemplary chosen pore sizes ranging between 10 and 60 Å and (b) changes in the pore space reflecting the mechanical flexibility in relation to the pore size.

https://doi.org/10.1021/acs.jpcc.4c07159
J. Phys. Chem. C 2024, 128, 21245−21252

deformed about 30% in volume after a compression of 15%, and then underwent negligible compression beyond. This indicates the hardening effect after the collapse of the smaller pores, and aligns very well with the detailed experimental study on carbon aerogels that showed that the smallest pores deformed the most under a given strain.[31] This shows that the nanostructured porous carbon remains flexible under finite deformations of up to 15% compressive strain. This is a very useful characteristic, making these materials attractive for applications such as cathode materials in lithium sulfur (Li−S) batteries, where the structure is subjected to cyclic deformation during charging and discharging under the influence of expansion and contraction of polysulfides infiltrated in the micropores of the material. The proposed model may serve as a good basis for simulating the mechanical deformation in the nanostructured porous carbon in Li−S batteries.

CONCLUSION

In summary, nanostructured porous carbon networks were successfully modeled using an all-atom molecular dynamics approach. The thermodynamic approach is used to model nanoporous carbon networks, starting from amorphous carbon. The method developed here was efficient in generating nanoporous carbon of various densities starting from 0.591 g cm^{-3} to as low as 0.144 g cm^{-3}. The radial distribution function gave insight into the C−C bonding and the connectivity of clusters with respect to the variation in the density of the model. The experimentally generated carbon aerogels were brittle and glassy in nature, with pores in the micro- and mesoporous ranges. The structure and pore-size distribution were calculated, along with the mechanical properties. The morphology, pore sizes, and the nonfractal nature of the studied model systems align well with the experimentally generated nanostructured carbon aerogels. The power scaling law between the Young modulus and the density exhibits a relation close to being quadratic, and was measured to be around 2.2. The mechanical flexibility was investigated by analyzing the effect of mechanical compression on the structure at different pore scales.

AUTHOR INFORMATION

Corresponding Author

Ameya Rege − *Institute of Materials Research, German Aerospace Center, 51147 Cologne, Germany; Department of Mechanics of Solids, Surfaces and Systems, University of Twente, 7500 AE Enschede, The Netherlands;* orcid.org/0000-0001-9564-5482; Email: ameya.rege@utwente.nl

Authors

Hemangi Patel − *Institute of Materials Research, German Aerospace Center, 51147 Cologne, Germany; Department of Chemistry, University of Cologne, 50939 Cologne, Germany*

Jessica Kröner − *Institute of Materials Research, German Aerospace Center, 51147 Cologne, Germany*

Marina Schwan − *Institute of Materials Research, German Aerospace Center, 51147 Cologne, Germany*

Barbara Milow − *Institute of Materials Research, German Aerospace Center, 51147 Cologne, Germany; Department of Chemistry, University of Cologne, 50939 Cologne, Germany*

Complete contact information is available at: https://pubs.acs.org/10.1021/acs.jpcc.4c07159

Notes

The authors declare no competing financial interest.

REFERENCES

(1) Biener, J.; Stadermann, M.; Suss, M.; Worsley, M. A.; Biener, M. M.; Rose, K. A.; Baumann, T. F. Advanced carbon aerogels for energy applications. *Energy Environ. Sci.* **2011**, *4*, 656−667.

(2) Nojabaee, M.; Sievert, B.; Schwan, M.; Schettler, J.; Warth, F.; Wagner, N.; Milow, B.; Friedrich, K. A. Ultramicroporous carbon aerogels encapsulating sulfur as the cathode for lithium-sulfur batteries. *Journal of Materials Chemistry A* **2021**, *9*, 6508−6519.

(3) Zuo, L.; Zhang, Y.; Zhang, L.; Miao, Y.-E.; Fan, W.; Liu, T. Polymer/carbon-based hybrid aerogels: preparation, properties and applications. *Materials* **2015**, *8*, 6806−6848.

(4) Smirnova, A.; Dong, X.; Hara, H.; Vasiliev, A.; Sammes, N. Novel carbon aerogel-supported catalysts for PEM fuel cell application. *International journal of hydrogen energy* **2005**, *30*, 149−158.

(5) Liang, C.; Li, Z.; Dai, S. Mesoporous carbon materials: synthesis and modification. *Angew. Chem., Int. Ed.* **2008**, *47*, 3696−3717.

(6) Pekala, R. Organic aerogels from the polycondensation of resorcinol with formaldehyde. *J. Mater. Sci.* **1989**, *24*, 3221−3227.

(7) Pekala, R. W.; Alviso, C. T. Carbon Aerogels and Xerogels. *MRS Proc.* **1992**, *270*, 3−14.

(8) Schwan, M.; Ratke, L. Flexible carbon aerogels. *C* **2016**, *2*, 22.

(9) Rege, A. A perspective on methods to computationally design the morphology of aerogels. *Adv. Eng. Mater.* **2023**, *25*, 2201097.

(10) Kieffer, J.; Angell, C. A. Generation of fractal structures by negative pressure rupturing of SiO2 glass. *J. Non-Cryst. Solids* **1988**, *106*, 336−342.

(11) Nakano, A.; Bi, L.; Kalia, R. K.; Vashishta, P. Structural correlations in porous silica: Molecular dynamics simulation on a parallel computer. *Physical review letters* **1993**, *71*, 85.

(12) Patil, S. P.; Rege, A.; Sagardas; Itskov, M.; Markert, B. Mechanics of nanostructured porous silica aerogel resulting from molecular dynamics simulations. *J. Phys. Chem. B* **2017**, *121*, 5660−5668.

(13) Wang, Y.; Fan, Z.; Qian, P.; Ala-Nissila, T.; Caro, M. A. Structure and pore size distribution in nanoporous carbon. *Chem. Mater.* **2022**, *34*, 617−628.

(14) Gavalda, S.; Kaneko, K.; Thomson, K. T.; Gubbins, K. E. Molecular modeling of carbon aerogels. *Colloids and surfaces A: Physicochemical and engineering aspects* **2001**, *187*, 531−538.

(15) Gavalda, S.; Gubbins, K.; Hanzawa, Y.; Kaneko, K.; Thomson, K. Nitrogen adsorption in carbon aerogels: A molecular simulation study. *Langmuir* **2002**, *18*, 2141−2151.

(16) Pang, H.-Q.; Li, S.; Li, Z.-Y. Grand canonical Monte Carlo simulations of hydrogen adsorption in carbon aerogels. *Int. J. Hydrogen Energy* **2021**, *46*, 34807−34821.

(17) Gor, G. Y.; Thommes, M.; Cychosz, K. A.; Neimark, A. V. Quenched solid density functional theory method for characterization of mesoporous carbons by nitrogen adsorption. *Carbon* **2012**, *50*, 1583−1590.

(18) Balzer, C.; Cimino, R. T.; Gor, G. Y.; Neimark, A. V.; Reichenauer, G. Deformation of microporous carbons during N2, Ar, and CO2 adsorption: Insight from the density functional theory. *Langmuir* **2016**, *32*, 8265−8274.

(19) Qin, Z.; Jung, G. S.; Kang, M. J.; Buehler, M. J. The mechanics and design of a lightweight three-dimensional graphene assembly. *Science Advances* **2017**, *3*, e1601536.

(20) Stuart, S. J.; Tutein, A. B.; Harrison, J. A. A reactive potential for hydrocarbons with intermolecular interactions. *J. Chem. Phys.* **2000**, *112*, 6472−6486.

(21) Brenner, D. W.; Shenderova, O. A.; Harrison, J. A.; Stuart, S. J.; Ni, B.; Sinnott, S. B. A second-generation reactive empirical bond order (REBO) potential energy expression for hydrocarbons. *J. Phys.: Condens. Matter* **2002**, *14*, 783.

(22) Thompson, A. P.; Aktulga, H. M.; Berger, R.; Bolintineanu, D. S.; Brown, W. M.; Crozier, P. S.; In't Veld, P. J.; Kohlmeyer, A.;

Moore, S. G.; Nguyen, T. D.; et al. LAMMPS-a flexible simulation tool for particle-based materials modeling at the atomic, meso, and continuum scales. *Comput. Phys. Commun.* **2022**, *271*, 108171.
(23) Seaton, N.; Walton, J.; et al. A new analysis method for the determination of the pore size distribution of porous carbons from nitrogen adsorption measurements. *Carbon* **1989**, *27*, 853−861.
(24) Ashby, M. F.; Gibson, L. J. *Cellular solids: structure and properties*; Press Syndicate of the University of Cambridge: Cambridge, UK, 1997; pp 175−231.
(25) Aney, S.; Pandit, P.; Ratke, L.; Milow, B.; Rege, A. On the origin of power-scaling exponents in silica aerogels. *J. Sol-Gel Sci. Technol.* **2023**, 1−8.
(26) Shiell, T. B.; Wong, S.; Yang, W.; Tanner, C. A.; Haberl, B.; Elliman, R. G.; McKenzie, D. R.; McCulloch, D. G.; Bradby, J. E. The composition, structure and properties of four different glassy carbons. *J. Non-Cryst. Solids* **2019**, *522*, 119561.
(27) Devreux, F.; Boilot, J.; Chaput, F.; Sapoval, B. NMR determination of the fractal dimension in silica aerogels. *Physical review letters* **1990**, *65*, 614.
(28) Rivas Murillo, J. S.; Bachlechner, M. E.; Campo, F. A.; Barbero, E. J. Structure and mechanical properties of silica aerogels and xerogels modeled by molecular dynamics simulation. *Journal of Non-Crystalline Solids* **2010**, *356*, 1325−1331.
(29) Abdusalamov, R.; Scherdel, C.; Itskov, M.; Milow, B.; Reichenauer, G.; Rege, A. Modeling and simulation of the aggregation and the structural and mechanical properties of silica aerogels. *J. Phys. Chem. B* **2021**, *125*, 1944−1950.
(30) Woignier, T.; Primera, J.; Alaoui, A.; Dieudonne, P.; Duffours, L.; Beurroies, I.; Calas-Etienne, S.; Despestis, F.; Faivre, A.; Etienne, P. Fractal structure in silica and composites aerogels. *Gels* **2021**, *7*, 1.
(31) Rege, A.; Schwan, M.; Chernova, L.; Hillgärtner, M.; Itskov, M.; Milow, B. Microstructural and mechanical characterization of carbon aerogels: An in-situ and digital image correlation-based study. *J. Non-Cryst. Solids* **2020**, *529*, 119568.

https://doi.org/10.1021/acs.jpcc.4c07159
J. Phys. Chem. C 2024, 128, 21245−21252